

Heralded Linear Optical Generation of Dicke States

Minhyeok Kang^{§1}, Jaehee Kim^{§1}, William J. Munro², Seungbeom Chin ^{*2}, and Joonsuk Huh ^{†3, 4}

¹SKKU Advanced Institute of Nanotechnology (SAINT), Sungkyunkwan University, Suwon 16419, Korea

²Okinawa Institute of Science and Technology Graduate University, Okinawa 904-0495, Japan

³Department of Chemistry, Yonsei University, Seoul 03722, Republic of Korea

⁴Department of Quantum Information, Yonsei University, Incheon 21983, Republic of Korea

December 25, 2025

Abstract

Entanglement is a fundamental feature of quantum mechanics and a key resource for quantum information processing. Among multipartite entangled states, Dicke states $|D_n^k\rangle$ are distinguished by their permutation symmetry, which provides robustness against particle loss and enables applications for quantum communication and computation. Although Dicke states have been realized in various platforms, most optical implementations rely on postselection, which destroys the state upon detection and prevents its further use. A heralded optical scheme is therefore highly desirable. Here, we present a linear-optical heralded scheme for generating arbitrary Dicke states $|D_n^k\rangle$ with $3n+k$ photons through the framework of the linear quantum graph (LQG) picture. By mapping the scheme design into the graph-finding problem, and exploiting the permutation symmetry of Dicke states, we overcome the structural complexity that has hindered previous approaches. Our results provide a resource-efficient pathway toward practical heralded preparation of Dicke states for quantum technologies.

1 Introduction

Entanglement is a fundamental feature of quantum mechanics, representing correlations with no classical reference. It not only plays a central role in deepening our understanding of the foundations of quantum theory, but also serves as the critical resource behind the advantages of quantum information processing [1]. Multipartite entanglement extends quantum correlations across many systems, enabling richer structures and more powerful applications than bipartite entanglement [2]. Such states are indispensable in areas including quantum cryptography [3–5], quantum teleportation [6–8], quantum dense coding [9–11], quantum error correction [12], and quantum computation [13, 14]. Over the past two decades, multipartite entanglement has been realized in diverse physical platforms—from trapped ions [15–17] and neutral atoms [18–20] to superconducting circuits [21–23], and photonic systems [24–27]—but scalable and resource-efficient generation of large entangled states still remains a central challenge.

Different classes of genuinely multipartite entangled states are characterized by distinct structures and applications [28, 29]. Dicke states $|D_n^k\rangle$ form one such class, defined as the equal-amplitude super-

^{*}sbthesy@gmail.com

[†]joonsukhuh@yonsei.ac.kr

[§]These authors contributed equally.

position of all computational basis states of n -qubits with Hamming weight k [30]:

$$|D_n^k\rangle = \sum_{\substack{\mathbf{x} \in \{0,1\}^{\otimes n} \\ \text{hw}(\mathbf{x})=k}} \binom{n}{k}^{-1/2} |\mathbf{x}\rangle. \quad (1)$$

Here, $\text{hw}(\mathbf{x})$ denotes the Hamming weight of the bitstring \mathbf{x} . Dicke states have a fixed number of qubit states ($n - k$ qubits of state 0 and k qubits of state 1) and are symmetric under qubit permutations, making them compactly representable within the symmetric subspace and resilient against particle loss. Their symmetry underlies applications across quantum networking [31], high-precision metrology [32–34], game theory [35], and error correction [36,37]. More recently, they have been recognized as efficient building blocks for variational quantum eigensolver (VQE) ansätze [38], enabling accurate simulations of many-body Hamiltonians with reduced resources.

Dicke states have been demonstrated experimentally in trapped ions [39–42], atomic systems [43–45], superconducting circuits [46] and optics [31, 47–50]. In photonics, they have been generated using diverse sources such as spontaneous parametric down-conversion (SPDC) [31, 47, 48], Cross-Kerr non-linearity [49], and single photon [50]. However, most previous works on Dicke state generation have relied on postselected methods—sorting out successful outcomes by detecting all photons—which irreversibly destroys the entanglement. Such states cannot then serve as resources in further quantum protocols. This limitation makes heralded optical generation of Dicke states an important open challenge.

Heralded schemes address this issue by using ancillary photons and modes as success signals, identifying valid runs without disturbing the target state. In principle, this preserves entanglement as a usable quantum resource. Yet, designing heralded schemes is significantly more difficult than postselected ones, since the required ancillas and correlations add structural complexity. To date, heralded generation of Dicke states has therefore remained elusive.

In this work, we propose a linear-optical heralded scheme that generates arbitrary Dicke states $|D_n^k\rangle$ within the linear quantum graph (LQG) picture [15,38,39]. The LQG framework maps physical components of entanglement-generating circuits into graph elements, reducing the problem of scheme design to that of graph construction. This approach has successfully yielded heralded schemes for GHZ, W, GHZ–W superpositions [39,40], caterpillar graph states [40], and qudit entangled states [41,42]. Here, we extend the LQG picture to Dicke states, embedding their intrinsic permutation symmetry directly into the graph structure. This reduces design complexity and enables systematic heralded constructions of arbitrary Dicke states. The resulting heralded Dicke state is compatible with existing photonic quantum platforms and can be employed as a genuine quantum resource.

This work is organized as follows: Section 2 reviews the LQG picture of sculpting protocol, the central tool we employ to construct our heralded scheme. Section 3 introduces the Dicke graph in LQG picture, which corresponds to a sculpting operator that generates $|D_n^k\rangle$. Section 4 demonstrates how the Dicke graph is implemented as a linear optical circuit that generates the Dicke state $|D_n^k\rangle$. Section 5 provides concluding remarks and discussions.

2 Review: LQG picture of the sculpting protocol

In this section, we review the concept of sculpting protocol as a operational process to generate multipartite entanglement, which can be mapped to balanced bipartite graphs or equivalently directed graphs [51,52].

Sculpting protocol.— We can generate n -partite entangled states in sculpting protocol by applying spatially overlapped $n+k$ single-boson annihilation operators (called “sculpting operators”) to a $2n+k$ boson initial state, where k is the number of ancillary modes. In our setup, each boson has an $n+k$ -dimensional spatial state and a two-dimensional internal state, hence creation and annihilation operators are expressed as $\hat{a}_{j,s}^\dagger$ and $\hat{a}_{j,s}$ ($j \in \{1, 2, \dots, n+k\}$, $s \in \{+, -\}$) respectively. Here we choose the computational basis in the x-direction for later convenience, which is expressed in the z-directional computation basis $\{|0\rangle, |1\rangle\}$ as $|\pm\rangle = (|0\rangle \pm |1\rangle)/\sqrt{2}$.

We consider a setup with n qubit systems and k ancillary systems. The initial state is given by

$$|\Psi_{\text{init}}\rangle_{n,k} = \prod_{j=1}^n \hat{a}_{j,+}^\dagger \hat{a}_{j,-}^\dagger \prod_{l=1}^k \hat{a}_{n+l,+}^\dagger |\text{vac}\rangle, \quad (2)$$

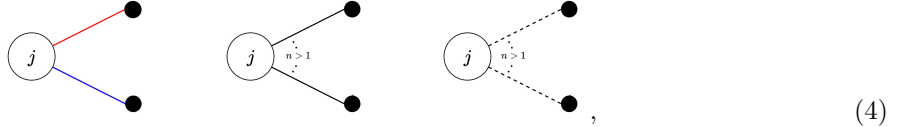
i.e., the n parties contain two bosons while k parties contain one boson. We apply a sculpting operator \hat{A}_{n+k} that subtracts $n+k$ bosons from $|\Psi_{\text{init}}\rangle_{n,k}$. The sculpting operator \hat{A}_{n+k} has the following form:

$$\hat{A}_{n+k} = \prod_{l=1}^{n+k} \hat{A}^{(l)} \equiv \prod_{l=1}^{n+k} \left(\sum_{j=1}^n (\alpha_j^{(l)} \hat{a}_{j,0} + \beta_j^{(l)} \hat{a}_{j,1}) + \sum_{m=1}^k \gamma_l^{(l)} \hat{a}_{n+l,+} \right) \quad (3)$$

with $\sum_{j=1}^n (|\alpha_j^{(l)}|^2 + |\beta_j^{(l)}|^2) + \sum_{m=1}^k |\gamma_l^{(m)}|^2 = 1$. For the above sculpting operator to generate a multipartite qubit state, the sculpting protocol must satisfy the *no-bunching restriction* [51], by which exactly one boson must be removed from each spatial mode by the operation of \hat{A}_{n+k} . Once we find a sculpting operator that generates an entangled state, it can be implemented in linear optics by translation rules [53].

LQG picture of sculpting protocols.— The LQG picture [51] maps all the essential elements in the sculpting protocol into graph elements. The same sculpting operator in the LQG picture can be described by two representations, the *undirected bigraph representation* (denoted as G_{ub}) and *directed unipartite graph representation* (denoted as G_{du}) [52]. Table 1 displays the correspondence relations from the physical elements of sculpting operator.

First, in the undirected bigraph representation G_{ub} , a sculpting operator is represented as an undirected balanced bipartite graph, which we call *sculpting bigraph*. For a sculpting operator to satisfy the no-bunching restriction, the final state must be completely determined by the superposition of the perfect matchings¹ of the corresponding sculpting bigraph [51]. Ref. [51] proposed a convenient subset of bigraphs—named *effective perfect matching bigraphs (EPM bigraphs)*—which inherently satisfy the no-bunching restriction by construction [51]. A bigraph is an EPM bigraph if all its edge-to-circle attachments match one of the configurations shown below:



where the edge colors {Solid Black, Dashed Black, Red, Blue} represent internal states $\{|+\rangle, |-\rangle, |0\rangle, |1\rangle\}$ ($|\pm\rangle = (|0\rangle \pm |1\rangle)/\sqrt{2}$). For an EPM bigraph in the LQG picture, we can show that the final state after the application of the corresponding sculpting operator is represented as the *superposition of all the perfect matchings of the EPM bigraph*.

¹A perfect matching of a graph $G = (V, E)$ is a subset of edges $M \subseteq E$ such that every vertex in V is incident to exactly one edge in M .

Table 1: Correspondence relations between a sculpting operator in bosonic systems and graphs in LQG picture. Since we work in the two computational bases $\{|0\rangle, |1\rangle\}$ and $\{|+\rangle, |-\rangle\}$ ($|\pm\rangle = (|0\rangle \pm |1\rangle)/\sqrt{2}$), the qubit states are represented as colors {Red, Blue} and {Solid Black, Dashed Black}.

Bosonic Systems with Sculpting Operator	Bipartite Graph $G = (U \cup V, E)$	Directed Graph $G = (W, E)$
Spatial modes j	Labelled circles (\circ_j)	Labelled circles (\circ_j)
$\hat{A}^{(l)}$	Unlabelled dots (\bullet)	Labelled circles (\circ_l)
Spatial distributions of \hat{A}_i	Undirected edges $\in E$	Directed edges $\in E$
Probability amplitude $\alpha_{i,j}, \beta_{i,j}, \gamma_{i,k}$	Edge weight $\alpha_{i,j}, \beta_{i,j}, \gamma_{i,k}$	Edge weight $\alpha_{i,j}, \beta_{i,j}, \gamma_{i,k}$
Qubit state ψ	Edge weight ψ (or color)	Edge weight ψ (or color)

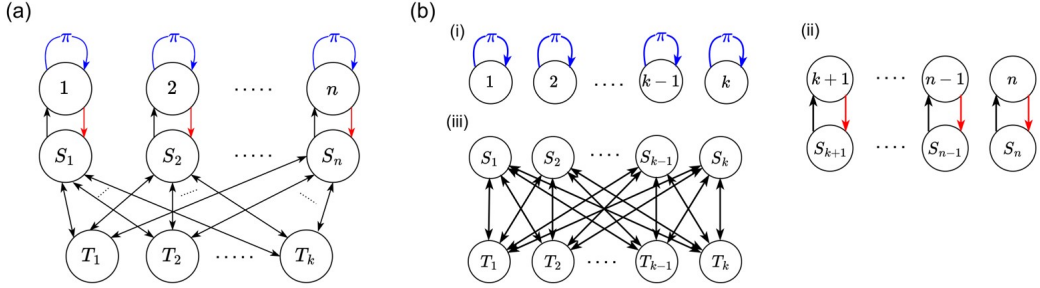
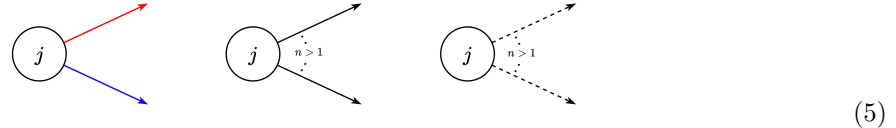


Figure 1: Dicke digraph D_n^k and its Directed Cycle Covers (DCCs). (a) The Dicke digraph D_n^k . Edge weights are omitted, implying that all outgoing edges from a vertex have equal amplitude weights. Two-headed arrows for $S_s \leftrightarrow A_a$ represent the combination of the two directed edges $S_s \rightarrow A_a$ and $A_a \rightarrow S_s$. (b) DCCs of D_n^k shown in (a). These include three types of cycles: (i) a system self-loop ($j \rightarrow j$); (ii) a 2-cycle on a system-ancilla pair ($S_j \rightarrow j \rightarrow S_j$); or (iii) an alternating $S \leftrightarrow T$ cycle of even length. The alternating cycles arise from the remaining vertices U and V forming a complete directed bipartite subgraph, where each choice of perfect matchings $S \rightarrow T$ and $T \rightarrow S$ specifies an alternating cycle cover.

Second, in the directed unipartite representation G_{du} , the same operator is represented as a directed graph, which we call *sculpting digraph*. A key concept in the digraph representation is the disjoint cycle cover² (DCC), which corresponds to a perfect matching in G_{ub} [26, 52, 54]. The final state is hence expressed as a superposition of all possible disjoint cycle covers in G_{du} . EPM bigraphs in G_{ub} are mapped to a special set of digraphs, of which edges are connected to circles as one of the following forms:



While G_{ub} is advantageous for intuitively illustrating sculpting protocols, G_{du} is more appropriate for visualizing complex entanglement structures, as we will see in the next section.

3 Dicke digraph D_n^k

In this section, we introduce the *Dicke digraph* D_n^k , which corresponds to a sculpting operator for generating Dicke states. We present it in the digraph representation G_{du} , because it directly reveals the symmetry of the operator in its structure.

Dicke digraph D_n^k is an EPM digraph that consists of n system vertices (denoted as $\{1, 2, \dots, n\}$) and $n+k$ ancillary vertices (denoted as S_j and T_l , where $j = 1, 2, \dots, n$ and $l = 1, 2, \dots, k$). We define two sets of ancillary vertices as $S \equiv \{S_j\}_{j=1}^n$ and $T \equiv \{T_l\}_{l=1}^k$. The ancillary vertices form a complete directed bipartite graph between S and T . And each system vertex j are connected to the corresponding ancillary vertex S_j . The most general form of D_n^k is shown in Fig. 1 (a). A key property of D_n^k is its symmetry: permutations of the pairs (j, S_j) among different j or of the T_l among l leave the graph invariant. Consequently, all disjoint cycle covers of D_n^k inherit this symmetry, ensuring that the generated quantum state shares the permutation symmetry of the Dicke state $|D_n^k\rangle$.

From Dicke graph to Dicke state.— From the structure of D_n^k , we can show that the final state generated by the corresponding sculpting operator is the Dicke state $|D_n^k\rangle$. To demonstrate this, we first check from Fig. 1 (a) that the Dicke digraph D_n^k is an EPM digraph (see (5)), hence the final state is the superposition of all its DCCs. Every cycle in D_n^k falls into one of three classes: a system self-loop

²A disjoint cycle cover of a digraph G is a collection of directed cycles such that every vertex of G lies in exactly one cycle.

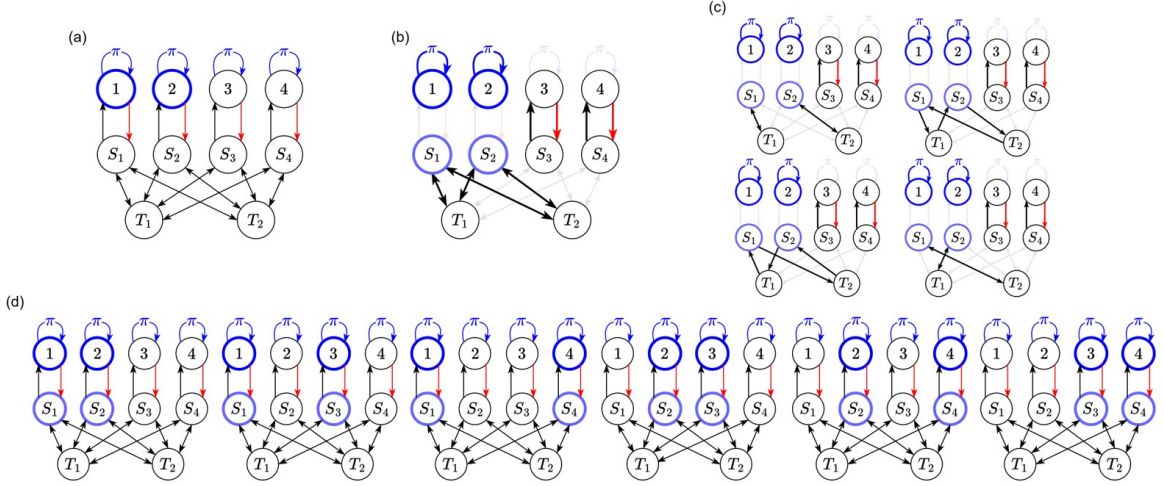


Figure 2: Example of the mechanism for the Dicke digraph with $(n, k) = (4, 2)$. (a) (b) The corresponding system vertices take self-loops, while the remaining system vertices form 2-cycles. $U = \{S_1, S_2\}$ and $W = \{T_1, T_2\}$ form a complete balanced directed bipartite subgraph. (c) Four disjoint cycle covers are possible in the subgraph, which correspond to the same operator monomial and generate $|1100\rangle$. (d) By the permutation symmetry among (j, S_j) ($j \in \{1, 2, 3, 4\}$) of the Dicke digraph, we can see that there are six more subgraphs that give permuted states of $|1100\rangle$, hence Dicke state $|D_4^2\rangle$.

$(j \rightarrow j)$, a 2-cycle $(j \rightarrow S_j \rightarrow j)$, or an cycle alternating through S and T , i.e., $S \leftrightarrow T$. Since system vertices are only connected to $\{S_j\}_{j=1}^n$ or itself, any cycle through j is either $(j \rightarrow j)$ or $(j \rightarrow S_j \rightarrow j)$; and each T_l is only connected to S , hence any cycle including T must be in $S \leftrightarrow T$. Then we can see that *all the DCCs contain $n - k$ self-loops* ($j \rightarrow j$), which is straightforward given that the elements in T are only connected to those in S and hence k elements in S are always included in the cycle $S \leftrightarrow T$.

Now let us consider the case when the system vertices $1, 2, \dots, k$ of the DCC have self-loops (see Fig. 1 (b)). Then the other system vertices $k+1, k+2, \dots, n$ are automatically included in $(j \rightarrow S_j \rightarrow j)$. The remaining cycles are those alternating between $U = \{S_1, \dots, S_k\}$ and $V = \{T_1, \dots, T_k\}$. Since the subgraph including S and T constructs a complete balanced bipartite graph, we can see that it has $(k!)^2$ distinct DCCs in it. From Table 1, we can directly see that these $(k!)^2$ DCCs with the same self-loops correspond to the same operator.

Indeed, the DCCs of the subgraph in Fig. 1 (b) are all written in the operator form as

$$\left(\prod_{m=1}^k -\hat{a}_{m,1} \right) \left(\prod_{p=k+1}^n \hat{a}_{p,0} \right) \left(\prod_{q=1}^n \hat{a}_{S_q,+} \right) \left(\prod_{l=1}^k \hat{a}_{T_l,+} \right). \quad (6)$$

This operator is applied to the $(3n + k)$ -particle initial state $|\Psi_{\text{init}}\rangle_{n,n+k}$ to obtain the state

$$\left(\prod_{m=1}^k \hat{a}_{m,1}^\dagger \right) \left(\prod_{p=k+1}^n \hat{a}_{p,0}^\dagger \right) |\text{vac}\rangle = |\underbrace{1, 1, \dots, 1}_k, \underbrace{0, 0, \dots, 0}_{n-k}\rangle, \quad (7)$$

which is directly derived using the identity

$$\hat{a}_{j,0} \hat{a}_{j,+}^\dagger \hat{a}_{j,-}^\dagger |\text{vac}\rangle = \hat{a}_{j,0}^\dagger |\text{vac}\rangle, \quad \hat{a}_{j,1} \hat{a}_{j,+}^\dagger \hat{a}_{j,-}^\dagger |\text{vac}\rangle = -\hat{a}_{j,1}^\dagger |\text{vac}\rangle. \quad (8)$$

By the permutation symmetry among the exchange of system qubits, the total final state becomes proportional to $|D_n^k\rangle$. By recovering all the normalization factors, the final state $|\Psi_{\text{fin}}\rangle$ is given by

$$|\Psi_{\text{fin}}\rangle = \hat{A}_{2n+k} |\Psi_{\text{init}}\rangle \sim |D_n^k\rangle |\text{vac}\rangle. \quad (9)$$

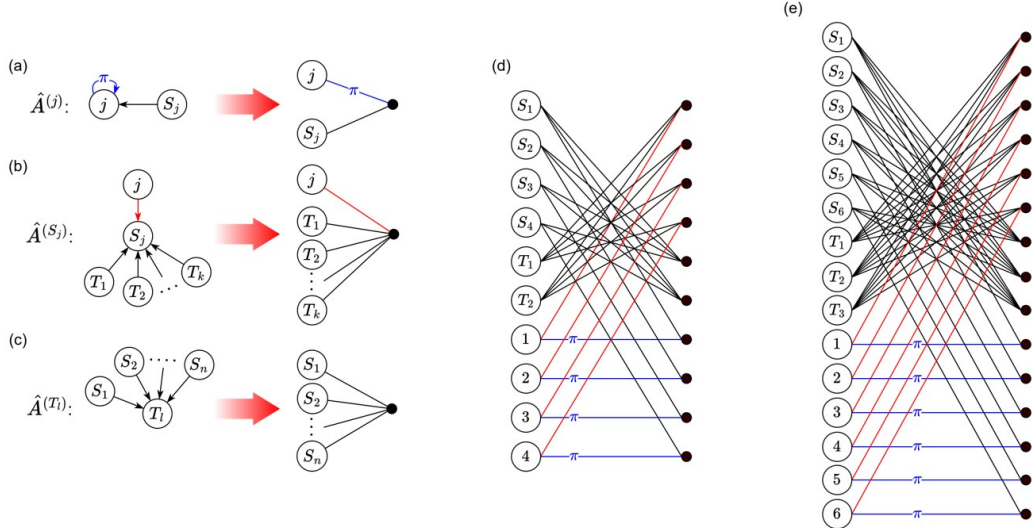


Figure 3: Conversion of a Dicke digraph into a sculpting bigraph. (a–c) Local subgraph transformation from G_{du} to G_{ub} . Node indices, colors and edge weights (including signs) are preserved. (d) Bigraphs D_4^2 and (e) D_6^3 constructed from the conversion.

D_4^2 example.— As a proof of concept, we analyze the simplest non-trivial $(n, k) = (4, 2)$ case here (see Fig. 2). First, we consider DCCs that have self-loops on 1 and 2 (Fig. 2 (a)). Then the other system vertices 3 and 4 pair with their corresponding ancillas to form the 2-cycles $(S_3 \rightarrow 3 \rightarrow S_3)$ and $(S_4 \rightarrow 4 \rightarrow S_4)$ (Fig. 2 (b)). Now the remaining vertices are $U = \{S_1, S_2\}$ and $V = \{T_1, T_2\}$; these induce a complete balanced bipartite directed graph. In $U \cup V$, a disjoint cycle cover is obtained by choosing one perfect matching for $S \rightarrow T$ and another independent perfect matching for $T \rightarrow S$, giving $(2!)^2 = 4$ possibilities (Fig. 2 (c)). These four DCCs all yield the same system operator monomial

$$\left(\prod_{m=1}^2 -\hat{a}_{m,1} \right) \left(\prod_{p=3}^4 \hat{a}_{p,0} \right) \left(\prod_{q=1}^4 \hat{a}_{S_q,+} \right) \left(\prod_{l=1}^2 \hat{a}_{T_l,+} \right). \quad (10)$$

Applying the above operator to the initial state

$$|\Psi_{\text{init}}\rangle_{4,6} = \prod_{j=1}^4 \hat{a}_{j,+}^\dagger \hat{a}_j^\dagger - \prod_{l=1}^4 \hat{a}_{S_l,+}^\dagger \prod_{m=1}^2 \hat{a}_{T_{m,+}}^\dagger |\text{vac}\rangle, \quad (11)$$

we obtain $|1100\rangle$. By the permutation symmetry among (j, S_j) ($j \in \{1, 2, 3, 4\}$) of the Dicke digraph, we can see that the final state is a superposition of the qubit permutation of $|1100\rangle$, hence becomes the Dicke state $|D_4^2\rangle$ (Fig. 2 (d)).

4 Heralded generation of Dicke states from Dicke graphs

In this section, based on the structure of D_n^k , we provide a physical setup that generates heralded Dicke states $|D_n^k\rangle$. While the sculpting protocol we propose can be implemented in any bosonic system with linear operations in principle, we present a linear optical circuit in this work. Following the procedure in Ref. [53], we design the circuit by first converting the Dicke digraph in G_{du} into an EPM bigraph in G_{ub} , and then mapping bigraph elements to optical elements via a set of translation rules. Those elements are assembled based on the structure of D_n^k , yielding the heralded circuit for our target state.

The transformation of D_n^k from G_{du} to G_{ub} is given in Fig. 3. The digraph D_n^k is decomposed into three elements denoted as $\hat{A}^{(j)}$, $\hat{A}^{(S_j)}$, and $\hat{A}^{(T_l)}$ in Fig. 3 (a)–(c). From the second column of Table 1, each elements are replaced with a dot connected to the relevant circles in G_{ub} . Those three elements completely compose the bigraph form of D_n^k for arbitrary n and k . Fig. 3 (d) displays the D_4^2 example.

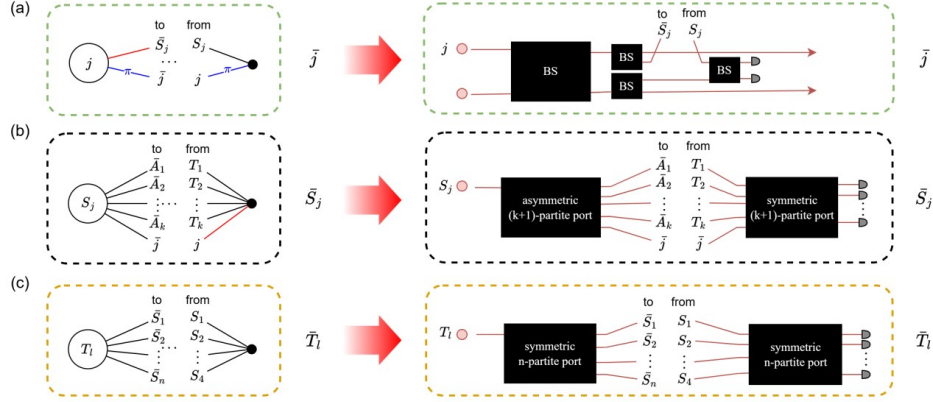


Figure 4: Transformation rules from bigraphs to linear optical networks. We decomposed D_n^k into circle-dot pairs on the same line in the bigraph. Each dashed box on the LHS is an open subgraph, whose open edges are attached to dots or circles following the designated labels. Then we obtain the circuit elements in the dotted boxes on the RHS from the translation rules in Fig. 2 of Ref. [53]. By connecting the open wires in the circuit elements, we can uniquely construct the linear optical circuit that generates $|D_n^k\rangle$ by heralding.

Then we can construct a linear optical setup following the translation rules from the bigraph elements to linear optical elements [53]. We adopt a dual-rail implementation using asymmetric and symmetric n -partite multiport interferometers, where the symmetric ones install the n -level discrete Fourier transformations (note that $n = 2$ multiport interferometer is the BS). In this architecture, each system mode m is represented as a dual-rail qubit composed of two spatial paths $(m, 0)$ and $(m, 1)$, corresponding to the logical states $|0_L\rangle$ and $|1_L\rangle$, respectively, while all ancillary and interface modes are treated as single-rail optical modes³. We then translate each circle-dot pair into linear optical components as shown in Fig. 4. Then the dashed boxes \bar{j} , \bar{S}_j and \bar{T}_l are connected to each other following the bigraph structure of D_n^k , hence we can uniquely construct a linear optical circuit for $|D_n^k\rangle$. For the simplest nontrivial $|D_4^2\rangle$ case, the circuit is as in Fig. 5.

Now we directly check that our circuit actually generates the target state, and derive the success probability by heralding. As denoted in Fig. 5, we divide the process into 5 steps:

Step 1. Preparation of the initial state as

$$\left(\prod_{j=1}^n \hat{a}_{S_j}^\dagger \right) \left(\prod_{l=1}^k \hat{a}_{T_l}^\dagger \right) \left(\prod_{m=1}^n \hat{a}_{m0}^\dagger \hat{a}_{m1}^\dagger \right). \quad (12)$$

Step 2. Division of the photon paths with BSs, asymmetric and symmetric multi-partite ports. Note that the number of paths divided from the ancillary modes corresponds to the number of edges for each ancillary vertex in the bigraph representation. The initial state as in Eq. (12) is transformed to

$$\frac{1}{2^n n^{k/2}} \left(\prod_{j=1}^n \left(\alpha \sum_{s=1}^k \hat{a}_{S_j s}^\dagger + \beta \hat{a}_{S_j k+1}^\dagger \right) \right) \cdot \left(\prod_{l=1}^k \left(\sum_{t=1}^n \hat{a}_{T_l t}^\dagger \right) \right) \cdot \left(\prod_{m=1}^n (\hat{a}_{m0}^{\dagger 2} - \hat{a}_{m1}^{\dagger 2}) \right). \quad (13)$$

Note that the probability amplitudes α and β ($|k|\alpha|^2 + |\beta|^2 = 1$) from asymmetric multiports are set to satisfy the symmetry of the circuit. We can control them so that the entire circuit can have the maximal success probability. We denote the creation operator of a mode split by the N -partite port or the BS from a given mode by adding additional indices, i.e., from $\hat{a}_{S_j}^\dagger$ to $\hat{a}_{S_j s}^\dagger$ with $s = 1, \dots, k+1$, and from $\hat{a}_{T_l}^\dagger$ to $\hat{a}_{T_l t}^\dagger$ with $t = 1, \dots, n$.

³Although the main derivation in the manuscript adopts this dual-rail implementation, the same construction can be equivalently realized using polarization encoding.

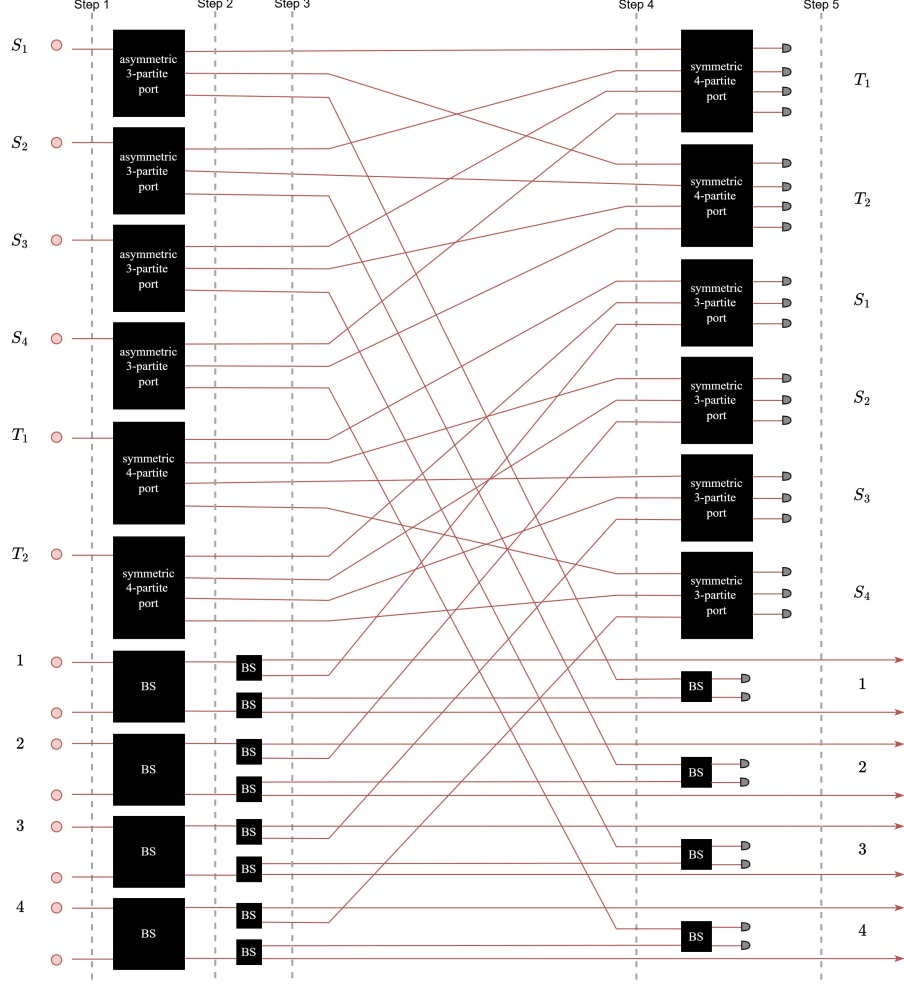


Figure 5: Linear optical network from Dicke digraph D_4^2 , split by several steps. Note that this figure is drawn with the positions of the 4-partite port and the 3-partite port swapped for clarity.

Step 3. Splitting two-photon states with BSs. By denoting the operator $\hat{a}_{j\sigma}^\dagger$ after the BS operation as $\hat{a}_{j\sigma\sigma'}^\dagger$ with $\sigma' = 0, 1$, the state evolves into

$$\begin{aligned} & \frac{1}{2^{2n}n^{k/2}} \left(\prod_{j=1}^n \left(\alpha \sum_{s=1}^k \hat{a}_{S_j s}^\dagger + \beta \hat{a}_{S_j k+1}^\dagger \right) \right) \cdot \left(\prod_{l=1}^k \left(\sum_{t=1}^n \hat{a}_{T_l t}^\dagger \right) \right) \\ & \times \left(\prod_{m=1}^n \left((\hat{a}_{m 0 0}^\dagger + \hat{a}_{m 0 1}^\dagger)^2 - (\hat{a}_{m 1 0}^\dagger - \hat{a}_{m 1 1}^\dagger)^2 \right) \right). \end{aligned} \quad (14)$$

Step 4. Permutation of wires. State (14) evolves into

$$\begin{aligned} & \frac{1}{2^{2n}n^{k/2}} \left(\prod_{j=1}^n \left(\alpha \hat{a}_{T_1 j}^\dagger + \dots + \alpha \hat{a}_{T_k j}^\dagger + \beta \hat{a}_{j 0 1}^\dagger \right) \right) \cdot \left(\prod_{l=1}^k \left(\hat{a}_{S_1 l}^\dagger + \dots + \hat{a}_{S_n l}^\dagger \right) \right) \\ & \times \left(\prod_{m=1}^n \left((\hat{a}_{m 0 0}^\dagger + \hat{a}_{S_m k+1}^\dagger)^2 - (\hat{a}_{m 1 0}^\dagger - \hat{a}_{m 1 1}^\dagger)^2 \right) \right). \end{aligned} \quad (15)$$

Step 5. Application of the n -partite port and BS before detection. Then (15) evolves into

$$\frac{1}{2^{2n}n^{k/2}} \left(\prod_{j=1}^n \left(\alpha \sum_{p=1}^n (U_n)_{pj} \hat{a}_{T_1 p}^\dagger + \cdots + \alpha \sum_{p=1}^n (U_n)_{pj} \hat{a}_{T_k p}^\dagger + \frac{\beta}{\sqrt{2}} (\hat{a}_{j01}^\dagger + \hat{a}_{j10}^\dagger) \right) \right) \quad (16)$$

$$\times \left(\prod_{l=1}^k \left(\sum_{q=1}^{k+1} (U_{k+1})_{ql} \hat{a}_{S_1 q}^\dagger + \cdots + \sum_{q=1}^{k+1} (U_{k+1})_{ql} \hat{a}_{S_n q}^\dagger \right) \right) \quad (17)$$

$$\times \left(\prod_{m=1}^n \left(\left(\hat{a}_{m00}^\dagger + \sum_{q=1}^{k+1} (U_{k+1})_{qk+1} \hat{a}_{S_m q}^\dagger \right)^2 - \left(\frac{1}{\sqrt{2}} (\hat{a}_{m01}^\dagger - \hat{a}_{m10}^\dagger) - \hat{a}_{m11}^\dagger \right)^2 \right) \right). \quad (18)$$

Here, U_d denotes the discrete Fourier transform matrix corresponding to a symmetric d -partite multiport.

After the postselection, all creation operators associated with the detected (upper-most) modes are removed, and only the non-detected modes remain. Collecting all $\binom{n}{k}$ possible combinations where k of the n modes correspond to the latter case gives the normalized post-selected state:

$$\binom{n}{k}^{-1/2} \sum_{\substack{M \subset \{1, \dots, n\} \\ |M|=k}} \left(\prod_{m \in M} \hat{a}_{m11}^\dagger \right) \left(\prod_{m \notin M} \hat{a}_{m00}^\dagger \right) |\text{vac}\rangle \quad (19)$$

with amplitude

$$\binom{n}{k}^{1/2} \frac{k!^2}{2^{\frac{3n}{2}} n^k (k+1)^{\frac{n}{2}}} \beta^{n-k} \alpha^k. \quad (20)$$

The factor $\beta^{n-k} \alpha^k$ attains its maximum value when

$$\beta = \sqrt{\frac{n-k}{n}}, \quad \alpha = \sqrt{\frac{1}{n}}. \quad (21)$$

Including the feed-forward factor $2^n n (k+1)$, the total success probability becomes

$$P_{\text{suc}} = \binom{n}{k} \frac{(k!)^4 (n-k)^{n-k}}{2^{2n} n^{n+2k-1} (k+1)^{n-1}}. \quad (22)$$

The success probabilities for $k = 2, 3, 4$ and n up to 10 are illustrated in Fig. 6 on a logarithmic scale. For $(n, k) = (4, 2)$, the success probability is about 3.4×10^{-6} which is compatible with current photonic technologies. The generation rates can be enhanced using temporal or spatial multiplexing of photon sources, parallelized detection, and fast feed-forward switching [55, 56]. These techniques make the scheme experimentally feasible within photonic quantum technologies.

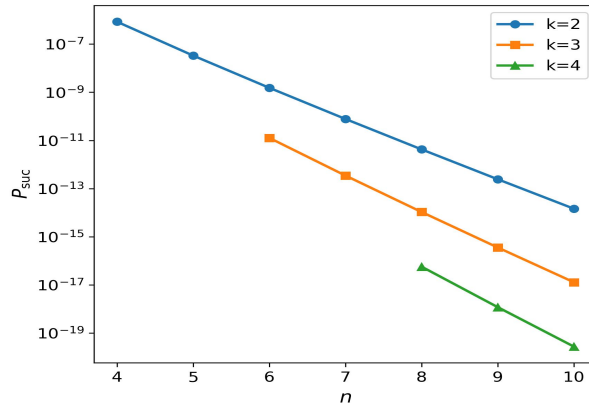


Figure 6: The success probability P_{suc} as a function of the n for $k = 2, 3, 4$. The probabilities are plotted on a logarithmic scale.

5 Conclusions

We have introduced a linear-optical heralded scheme for generating Dicke states within the linear quantum graph picture, overcoming the limitations of postselected approaches. By encoding the inherent permutation symmetry of Dicke states into graph structures, we substantially simplify the design problem and obtain systematic heralded schemes. Our result is compatible with current photonic technologies, with significantly higher success probabilities above detector dark-count levels. To our knowledge, no prior heralded linear optical scheme for generating Dicke states with feedforward has been reported.

The intrinsic robustness of Dicke states to particle loss indicates the possibility of developing loss-tolerant or application-optimized variants tailored to quantum networking, distributed sensing, and photonic variational algorithms. These directions position our scheme as a stepping stone toward practical multi-photon resource generation in future quantum technologies. Our work also highlights the usefulness of the LQG framework for discovering heralded entanglement generation schemes. Future research extends this approach to other highly symmetric and practically relevant resource states, including families of stabilizer states and absolutely maximally entangled states.

Acknowledgments

MK, JK, and JH are supported by National Research Foundation of Korea (NRF, RS-2023-NR068116, RS-2023-NR119931, RS-2025-03532992), Institute for Information & Communications Technology Promotion (IITP) grant funded by the Korea government (MSIP) (No. 2019-0-00003), and Yonsei University Research Fund under project number 2025-22-0140. SC is supported by National Research Foundation of Korea (NRF, RS-2023-00245747). WJM was partially supported by the JSPS Kakenhi Grant No. 21H04880.

References

- [1] Ryszard Horodecki, Paweł Horodecki, Michał Horodecki, and Karol Horodecki. Quantum entanglement. *Rev. Mod. Phys.*, 81:865–942, Jun 2009.
- [2] Michael Walter, David Gross, and Jens Eisert. Multipartite entanglement. *Quantum Information: From Foundations to Quantum Technology Applications*, pages 293–330, 2016.
- [3] Artur K. Ekert. Quantum cryptography based on Bell’s theorem. *Phys. Rev. Lett.*, 67:661–663, Aug 1991.
- [4] Massimiliano Proietti, Joseph Ho, Federico Grasselli, Peter Barrow, Mehul Malik, and Alessandro Fedrizzi. Experimental quantum conference key agreement. *Science Advances*, 7(23):eabe0395, 2021.
- [5] Gláucia Murta, Federico Grasselli, Hermann Kampermann, and Dagmar Bruß. Quantum Conference Key Agreement: A Review. *Advanced Quantum Technologies*, 3(11), 2020.
- [6] Charles H. Bennett, Gilles Brassard, Claude Crépeau, Richard Jozsa, Asher Peres, and William K. Wootters. Teleporting an unknown quantum state via dual classical and einstein-podolsky-rosen channels. *Phys. Rev. Lett.*, 70:1895–1899, Mar 1993.
- [7] Yi-Han Luo, Han-Sen Zhong, Manuel Erhard, Xi-Lin Wang, Li-Chao Peng, Mario Krenn, Xiao Jiang, Li Li, Nai-Le Liu, Chao-Yang Lu, Anton Zeilinger, and Jian-Wei Pan. Quantum Teleportation in High Dimensions. *Physical Review Letters*, 123(7):070505, 2019.
- [8] S. L. N. Hermans, M. Pompili, H. K. C. Beukers, S. Baier, J. Borregaard, and R. Hanson. Qubit teleportation between non-neighbouring nodes in a quantum network. *Nature*, 605(7911):663–668, 2022.
- [9] Charles H. Bennett and Stephen J. Wiesner. Communication via one- and two-particle operators on Einstein-Podolsky-Rosen states. *Phys. Rev. Lett.*, 69:2881–2884, Nov 1992.

[10] Yu Guo, Bi-Heng Liu, Chuan-Feng Li, and Guang-Can Guo. Advances in Quantum Dense Coding. *Advanced Quantum Technologies*, 2(5-6), 2019.

[11] Xiao-Min Hu, Yu Guo, Bi-Heng Liu, Yun-Feng Huang, Chuan-Feng Li, and Guang-Can Guo. Beating the channel capacity limit for superdense coding with entangled ququarts. *Science Advances*, 4(7):eaat9304, 2018.

[12] Google Quantum AI et al. Suppressing quantum errors by scaling a surface code logical qubit. *Nature*, 614(7949):676–681, 2023.

[13] Dolev Bluvstein, Simon J. Evered, Alexandra A. Geim, Sophie H. Li, Hengyun Zhou, Tom Manovitz, Sepehr Ebadi, Madelyn Cain, Marcin Kalinowski, Dominik Hangleiter, J. Pablo Bonilla Ataides, Nishad Maskara, Iris Cong, Xun Gao, Pedro Sales Rodriguez, Thomas Karolyshyn, Giulia Semeghini, Michael J. Gullans, Markus Greiner, Vladan Vuletić, and Mikhail D. Lukin. Logical quantum processor based on reconfigurable atom arrays. *Nature*, 626(7997):58–65, 2024.

[14] Lars S. Madsen, Fabian Laudenbach, Mohsen Falamarzi. Askarani, Fabien Rortais, Trevor Vincent, Jacob F. F. Bulmer, Filippo M. Miatto, Leonhard Neuhaus, Lukas G. Helt, Matthew J. Collins, Adriana E. Lita, Thomas Gerrits, Sae Woo Nam, Varun D. Vaidya, Matteo Menotti, Ish Dhand, Zachary Vernon, Nicolás Quesada, and Jonathan Lavoie. Quantum computational advantage with a programmable photonic processor. *Nature*, 606(7912):75–81, 2022.

[15] Dietrich Leibfried, Emanuel Knill, Signe Seidelin, Joe Britton, R Brad Blakestad, John Chiaverini, David B Hume, Wayne M Itano, John D Jost, Christopher Langer, et al. Creation of a six-atom ‘Schrödinger cat’ state. *Nature*, 438(7068):639–642, 2005.

[16] DB Hume, Till Rosenband, and David J Wineland. High-fidelity adaptive qubit detection through repetitive quantum nondemolition measurements. *Physical review letters*, 99(12):120502, 2007.

[17] Thomas Monz, Philipp Schindler, Julio T Barreiro, Michael Chwalla, Daniel Nigg, William A Coish, Maximilian Harlander, Wolfgang Hänsel, Markus Henrich, and Rainer Blatt. 14-qubit entanglement: Creation and coherence. *Physical Review Letters*, 106(13):130506, 2011.

[18] Olaf Mandel, Markus Greiner, Artur Widera, Tim Rom, Theodor W Hänsch, and Immanuel Bloch. Controlled collisions for multi-particle entanglement of optically trapped atoms. *Nature*, 425(6961):937–940, 2003.

[19] Hannes Bernien, Sylvain Schwartz, Alexander Keesling, Harry Levine, Ahmed Omran, Hannes Pichler, Soonwon Choi, Alexander S Zibrov, Manuel Endres, Markus Greiner, et al. Probing many-body dynamics on a 51-atom quantum simulator. *Nature*, 551(7682):579–584, 2017.

[20] Ahmed Omran, Harry Levine, Alexander Keesling, Giulia Semeghini, Tout T Wang, Sepehr Ebadi, Hannes Bernien, Alexander S Zibrov, Hannes Pichler, Soonwon Choi, et al. Generation and manipulation of Schrödinger cat states in Rydberg atom arrays. *Science*, 365(6453):570–574, 2019.

[21] Matthew Neeley, Radoslaw C Bialczak, M Lenander, Erik Lucero, Matteo Mariantoni, AD O’connell, D Sank, H Wang, M Weides, J Wenner, et al. Generation of three-qubit entangled states using superconducting phase qubits. *Nature*, 467(7315):570–573, 2010.

[22] Leonardo DiCarlo, Matthew D Reed, Luyan Sun, Blake R Johnson, Jerry M Chow, Jay M Gambetta, Luigi Frunzio, Steven M Girvin, Michel H Devoret, and Robert J Schoelkopf. Preparation and measurement of three-qubit entanglement in a superconducting circuit. *Nature*, 467(7315):574–578, 2010.

[23] Chao Song, Kai Xu, Wuxin Liu, Chui-ping Yang, Shi-Biao Zheng, Hui Deng, Qiwei Xie, Keqiang Huang, Qiujiang Guo, Libo Zhang, et al. 10-qubit entanglement and parallel logic operations with a superconducting circuit. *Physical review letters*, 119(18):180511, 2017.

[24] Dik Bouwmeester, Jian-Wei Pan, Matthew Daniell, Harald Weinfurter, and Anton Zeilinger. Observation of three-photon greenberger-horne-zeilinger entanglement. *Phys. Rev. Lett.*, 82:1345–1349, Feb 1999.

[25] Chao-Yang Lu, Xiao-Qi Zhou, Otfried Gühne, Wei-Bo Gao, Jin Zhang, Zhen-Sheng Yuan, Alexander Goebel, Tao Yang, and Jian-Wei Pan. Experimental entanglement of six photons in graph states. *Nature Physics*, 3(2):91–95, Feb 2007.

[26] Seungbeom Chin, Yong-Su Kim, and Sangmin Lee. Graph Picture of Linear Quantum Networks and Entanglement. *Quantum*, 5:611, 2021.

[27] Donghwa Lee, Tanumoy Pramanik, Seongjin Hong, Young-Wook Cho, Hyang-Tag Lim, Seungbeom Chin, and Yong-Su Kim. Entangling three identical particles via spatial overlap. *Optics Express*, 30(17):30525–30535, 2022.

[28] Wolfgang Dür, Guifre Vidal, and J Ignacio Cirac. Three qubits can be entangled in two inequivalent ways. *Physical Review A*, 62(6):062314, 2000.

[29] Mengru Ma, Yinfei Li, and Jiangwei Shang. Multipartite entanglement measures: A review. *Fundamental Research*, 2024.

[30] R. H. Dicke. Coherence in spontaneous radiation processes. *Phys. Rev.*, 93:99–110, Jan 1954.

[31] R. Prevedel, G. Cronenberg, M. S. Tame, M. Paternostro, P. Walther, M. S. Kim, and A. Zeilinger. Experimental realization of Dicke states of up to six qubits for multiparty quantum networking. *Phys. Rev. Lett.*, 103:020503, Jul 2009.

[32] Géza Tóth. Multipartite entanglement and high-precision metrology. *Phys. Rev. A*, 85:022322, Feb 2012.

[33] Yingkai Ouyang, Nathan Shettell, and Damian Markham. Robust quantum metrology with explicit symmetric states. *IEEE Transactions on Information Theory*, 68(3):1809–1821, 2022.

[34] Zain H. Saleem, Michael Perlin, Anil Shaji, and Stephen K. Gray. Achieving the Heisenberg limit with Dicke states in noisy quantum metrology. *Phys. Rev. A*, 109:052615, May 2024.

[35] S K Özdemir, J Shimamura, and N Imoto. A necessary and sufficient condition to play games in quantum mechanical settings. *New Journal of Physics*, 9(2):43, feb 2007.

[36] Yingkai Ouyang. Permutation-invariant quantum codes. *Phys. Rev. A*, 90:062317, Dec 2014.

[37] Arda Aydin, Max A. Alekseyev, and Alexander Barg. A family of permutationally invariant quantum codes. *Quantum*, 8:1321, April 2024.

[38] José Victor S Scursulim, Gabriel Mattos Langeloh, Victor Leme Beltran, and Samuráí Brito. Multiclass Portfolio Optimization via Variational Quantum Eigensolver with Dicke State Ansatz. *arXiv preprint arXiv:2508.13954*, 2025.

[39] I. E. Linington and N. V. Vitanov. Robust creation of arbitrary-sized Dicke states of trapped ions by global addressing. *Phys. Rev. A*, 77:010302, Jan 2008.

[40] D. B. Hume, C. W. Chou, T. Rosenband, and D. J. Wineland. Preparation of Dicke states in an ion chain. *Phys. Rev. A*, 80:052302, Nov 2009.

[41] Svetoslav S Ivanov, Nikolay V Vitanov, and Natalia V Korolkova. Creation of arbitrary Dicke and NOON states of trapped-ion qubits by global addressing with composite pulses. *New Journal of Physics*, 15(2):023039, feb 2013.

[42] L. Lamata, C. E. López, B. P. Lanyon, T. Bastin, J. C. Retamal, and E. Solano. Deterministic generation of arbitrary symmetric states and entanglement classes. *Phys. Rev. A*, 87:032325, Mar 2013.

[43] John K. Stockton, Ramon van Handel, and Hideo Mabuchi. Deterministic dicke-state preparation with continuous measurement and control. *Phys. Rev. A*, 70:022106, Aug 2004.

[44] Yun-Feng Xiao, Xu-Bo Zou, and Guang-Can Guo. Generation of atomic entangled states with selective resonant interaction in cavity quantum electrodynamics. *Phys. Rev. A*, 75:012310, Jan 2007.

[45] Xiao-Qiang Shao, Li Chen, Shou Zhang, Yong-Fang Zhao, and Kyu-Hwang Yeon. Deterministic generation of arbitrary multi-atom symmetric Dicke states by a combination of quantum zeno dynamics and adiabatic passage. *Europhysics Letters*, 90(5):50003, jun 2010.

[46] Chunfeng Wu, Chu Guo, Yimin Wang, Gangcheng Wang, Xun-Li Feng, and Jing-Ling Chen. Generation of dicke states in the ultrastrong-coupling regime of circuit qed systems. *Phys. Rev. A*, 95:013845, Jan 2017.

[47] N. Kiesel, C. Schmid, G. Tóth, E. Solano, and H. Weinfurter. Experimental observation of four-photon entangled Dicke state with high fidelity. *Phys. Rev. Lett.*, 98:063604, Feb 2007.

[48] Witlef Wieczorek, Roland Krischek, Nikolai Kiesel, Patrick Michelberger, Géza Tóth, and Harald Weinfurter. Experimental entanglement of a six-photon symmetric dicke state. *Phys. Rev. Lett.*, 103:020504, Jul 2009.

[49] Chunran Zhao and Liu Ye. Efficient scheme for the preparation of symmetric Dicke states via cross-kerr nonlinearity. *Physics Letters A*, 375(3):401–405, 2011.

[50] Sachin Kasture. Scalable approach to generation of large symmetric Dicke states. *Phys. Rev. A*, 97(4):043862, Apr 2018.

[51] Seungbeom Chin, Yong-Su Kim, and Marcin Karczewski. Shortcut to multipartite entanglement generation: A graph approach to boson subtractions. *npj Quantum Information*, 10(1):67, 2024.

[52] Seungbeom Chin and William J. Munro. Efficient Photonic Graph State Generation. *arXiv preprint arXiv:2306.15148*, 2023.

[53] Seungbeom Chin, Marcin Karczewski, and Yong-Su Kim. Heralded Optical Entanglement Generation via the Graph Picture of Linear Quantum Networks. *Quantum*, 8:1572, 2024.

[54] W. T. Tutte. A short proof of the factor theorem for finite graphs. *Canadian Journal of Mathematics*, 6(0):347–352, 1954.

[55] Evan Meyer-Scott, Christine Silberhorn, and Alan Migdall. Single-photon sources: Approaching the ideal through multiplexing. *Review of Scientific Instruments*, 91(4), 2020.

[56] Philip J Bustard, Ramy Tannous, Kent Bonsma-Fisher, Daniel Poitras, Cyril Hnatovsky, Stephen J Mihailov, Duncan England, and Benjamin J Sussman. Toward deterministic sources: Photon generation in a fiber-cavity quantum memory. *Physical Review A*, 109(1):013711, 2024.